ASN NEURO RESEARCH ARTICLE

ASN NEURO 4(6):art:e00100.doi:10.1042/AN20120062

Astrogliosis during acute and chronic cuprizone demyelination and implications for remyelination

Norah Hibbits*[1], Jun Yoshino[†1], Tuan Q. Le[‡] and Regina C. Armstrong*[,‡2]

*Neuroscience Program, Uniformed Services University of Health Sciences 4301 Jones Bridge Road Bethesda, MD 20814, U.S.A.

[†]Department of Psychology and Program of Neuroscience Colgate University Hamilton, NY 13346, U.S.A.

[‡]Department of Anatomy, Physiology, and Genetics, Uniformed Services University of Health Sciences 4301 Jones Bridge Road Bethesda, MD 20814, U.S.A.

Cite this article as: Hibbits N, Yoshino J, Le TQ and Armstrong RC (2012) Astrogliosis during acute and chronic cuprizone demyelination and implications for remyelination. ASN NEURO 4(6):art:e00100.doi:10.1042/AN20120062

ABSTRACT

In multiple sclerosis, microglia/macrophage activation and astrocyte reactivity are important components of the lesion environment that can impact remyelination. The current study characterizes these glial populations relative to expression of candidate regulatory molecules in cuprizone demyelinated corpus callosum. Importantly, periods of recovery after acute or chronic cuprizone demyelination are examined to compare conditions of efficient versus limited remyelination, respectively. Microglial activation attenuates after early demyelination. In contrast, astrocyte reactivity persists throughout demyelination and a 6-week recovery period following either acute or chronic demyelination. This astrocyte reaction is characterized by (a) early proliferation, (b) increased expression of GFAP (glial fibrillary acidic protein), Vim (vimentin), Fn1 (fibronectin) and CSPGs (chondroitin sulphate proteoglycans) and (c) elaboration of a dense network of processes. Glial processes elongated in the axonal plane persist throughout lesion areas during both the robust remyelination that follows acute demyelination and the partial remyelination that follows chronic demyelination. However, prolonged astrocyte reactivity with chronic cuprizone treatment does not progress to barrier formation, i.e. dense compaction of astrocyte processes to wall off the lesion area. Multiple candidate growth factors and inflammatory signals in the lesion environment show strong correlations with GFAP across the acute cuprizone demyelination and recovery time course, yet there is more divergence across the progression of chronic cuprizone demyelination and recovery. However, differential glial scar formation does not appear to be responsible for differential remyelination during recovery in the cuprizone model. The astrocyte phenotype and lesion characteristics in this demyelination model inform studies to identify triggers of non-remyelinating sclerosis in chronic multiple sclerosis lesions.

Key words: astrocyte, extracellular matrix, glial scar, growth factor, multiple sclerosis.

INTRODUCTION

Glial cells are exquisitely sensitive to CNS (central nervous system) damage. The complex reactions of astrocytes and microglia are key components of the pathological environment. Astrocytes, more so than microglia, are associated with tissue modifications that form barriers to regeneration, such as axon growth and remyelination (Sofroniew and Vinters, 2010). In demyelinating diseases, the progression of astrocyte reactivity and the associated regulatory signalling in the lesion environment that inhibit remyelination are poorly understood.

In the demyelinating disease multiple sclerosis, astrocyte scar formation is considered a prominent feature of the sclerotic lesions observed in chronic cases. Furthermore, remyelinating and non-remyelinating regions of multiple sclerosis lesions exhibit differential astroglial phenotypes (John et al., 2002; Nair et al., 2008). Inflammatory mediators in this autoimmune disease can induce reactive changes in astrocytes (John et al.,

[1] These authors contributed equally to this work.

[2] To whom correspondence should be addressed (email regina.armstrong@usuhs.edu).

Abbreviations: BMP4, bone morphogenetic protein 4; CNS, central nervous system; CSPG, chondroitin sulfate proteoglycan; C_t, threshold cycle; Cy3, indocarbocyanine; FGF2, fibroblast growth factor 2; Fn1, fibronectin; GAG, glycosaminoglycan; GFAP, glial fibrillary acidic protein; Glu1, glutamine synthetase; IGF-1, insulin-like growth factor 1; IL-1β, interleukin 1β; Itgam, integrin alpha M; LIF, leukaemia inhibitory factor; LPS, lipopolysaccharide; MCAO, middle cerebral artery occlusion; MOG, myelin oligodendrocyte glycoprotein; Nes, nestin; PFA, paraformaldehyde; Plp1, proteolipid protein; Ptprz1, phosphacan; QPCR, quantitative PCR; TGFβ, transforming growth factor β; TnC, tenascin C; TNFα, tumour necrosis factor α; Vim, vimentin.

2005). Breakdown of the blood–brain barrier can also stimulate astrocyte reactivity. Inflammation and blood–brain barrier leakage are associated with active multiple sclerosis disease stages. It is not clear how these processes may contribute to the phenotype of astrocytes associated with non-remyelinating, sclerotic lesions of chronic, inactive multiple sclerosis lesions. It is also not known whether the duration of astrocyte reactivity influences the astrocyte phenotype and progression of sclerosis in chronic lesions.

The cuprizone neurotoxicant model of experimental demyelination is advantageous for characterizing the glial response during prolonged demyelination and differential remyelination. Cuprizone ingestion causes oligodendrocyte loss and microglial activation without a marked lymphocytic response (Matsushima and Morell, 2001). These pathological features are similar to pattern III lesions of multiple sclerosis (Lucchinetti et al., 1999). Early microglial activation initiates a cascade of signals that stimulates astrocytes to express signalling molecules which contribute to demyelination, indicating a key role of reactive astrocytes in the progression of demyelinating disease (Kang et al., 2012). The ability to remove the demyelinating agent simplifies studies of the remyelination phase. When used as a short-term protocol, cuprizone produces a single episode of 'acute' demyelination followed by efficient spontaneous remyelination. More prolonged cuprizone ingestion results in a continuous 'chronic' demyelination state which subsequently remyelinates poorly. Therefore cuprizone can facilitate comparison of the tissue environments associated with efficient against limited remyelination (Armstrong et al., 2006; Mason et al., 2004).

Astrogliosis in the cuprizone model has typically been characterized using immunohistochemical detection of GFAP (glial fibrillary acidic protein) either to count the number of astrocytes or measure immunoreactivity in a region of interest. Astroglial activation begins during initial stages of cuprizone demyelination (Buschmann et al., 2012; Hiremath et al., 1998) and continues through at least 12 weeks of cuprizone ingestion (Kipp et al., 2011; Lindner et al., 2009; Plant et al., 2005; Xie et al., 2010). Following acute demyelination, GFAP expression remains elevated for several weeks (Plant et al., 2005). However, the astroglial response to injury is much more complex than GFAP staining intensity or astrocyte cell number can capture. More thorough characterization of the astroglial reaction is required. Astroglial characteristics may be especially important in the cuprizone model with respect to environmental features that influence differential remyelination following acute versus chronic cuprizone. Therefore studies are needed to phenotype the astrocytic response in the period after removal of cuprizone from the diet.

The current studies characterize microglial activation and astrogliosis throughout acute and chronic cuprizone demyelination with a focus on the subsequent recovery periods on normal chow. We find that astrocyte reactivity, in contrast with microglial activation, continues during chronic demyelination and through a 6-week recovery period to allow for remyelination. A battery of immunohistochemical and histological indicators is used to phenotype the astrocytic response. QPCR (quantitative PCR) gene arrays further characterize the pattern of genes expressed in the corpus callosum throughout the periods of cuprizone treatment and recovery. These arrays include analysis of indicators of astrogliosis and candidate genes in the lesion environment that may stimulate astroglial responses and/or regulate the extent of remyelination. These QPCR arrays are the first to examine expression patterns of environmental signals for comparison between recovery periods with distinctly different remyelination efficiencies, i.e. robust remyelination after an acute episode of cuprizone demyelination as compared with limited remyelination capacity after more prolonged cuprizone treatment.

METHODS

Cuprizone model

The cuprizone model was performed as in our previous studies of short- and long-term administration protocols (Armstrong et al., 2006; Vana et al., 2007; Zhou et al., 2012). Male C57BL/6 mice (6–7 weeks of age) were purchased from Jackson Laboratories and housed two per cage on a 12 h light–dark cycle at the Uniformed Services Health Sciences animal facility. Food and water were provided *ad libitum*. To induce demyelination, 8-week-old mice were fed a 0.2% (w/w) cuprizone diet [finely powdered oxalic bis(cyclohexylidenehydrazide); Sigma-Aldrich] mixed into milled chow (Certified LM-485 code 7012CM; Harlan Teklad). Mice were fed cuprizone continuously for either 6 weeks for 'acute' or 12 weeks for 'chronic' demyelination models. After cuprizone feeding, mice were returned to normal chow for either 3- or 6-week periods to evaluate spontaneous recovery. Control mice were fed normal chow without cuprizone and analysed at ages matched to the start of cuprizone (8 weeks) and the end points of each time course for 6 weeks of cuprizone and 6 weeks of recovery (20 weeks) or 12 weeks of cuprizone and 6 weeks of recovery (26 weeks).

Analysis of tissue sections

Mice were perfused with 4% PFA (paraformaldehyde) and brains were dissected prior to overnight post fixation in 4% PFA. Brains were then cryoprotected in 30% sucrose overnight, embedded in Tissue Tek OCT, and stored at −80°C. For immunohistochemical analysis, 15 μm coronal sections were cut and mounted on Superfrost Plus slides.

MOG (myelin oligodendrocyte glycoprotein) was detected with the monoclonal antibody 8–18C5 (Dr Minettia Gardinier, Department of Pharmacology, University of Iowa, Iowa City, IA U.S.A.). GFAP was detected using a rabbit polyclonal IgG

antibody (DAKO). In combination with GFAP immunostaining, Ki67 was detected following heating in Antigen Retrieval Citra Solution (Biogenex). Vim (vimentin) was detected using a mouse monoclonal antibody (Millipore). Fn1 (fibronectin) was detected using a rabbit anti-Fn1 antibody (Chemicon, Millipore). A mouse monoclonal anti-chondroitin sulphate antibody (Clone CS-56, Sigma) was used to immunostain the GAG (glycosaminoglycan) moiety of CSPGs (chondroitin sulphate proteoglycans). DSD-1 is the mouse homologue of rat Ptprz1 (phosphacan) and was detected with a monoclonal against DSD-1 (Millipore). Anti-CD11b (Abcam) was used to identify microglia/macrophage cells. Anti-CD36 (Abcam) was used to identify endothelial cells of blood vessels. Primary antibodies were detected with Alexa Fluor® 555-conjugated goat anti-rat IgG, Alexa Fluor® 488-conjugated goat anti-rabbit IgG (Invitrogen), Cy3 (indocarbocyanine)-conjugated donkey anti-mouse IgG F(ab)$_2$ (Jackson Immunoresearch), or Cy3-conjugated donkey anti-mouse IgM (Jackson Immunoresearch). For collagen histology, paraffin sections were stained using Masson's Trichrome Blue (Sigma) stain to detect collagen fibres. Corpus callosum myelination status and astrogliosis was estimated based on the area of MOG or GFAP immunostaining, respectively, quantified in coronal sections (Armstrong et al., 2006). An index of proliferation was determined by counting all Ki67 immunolabelled nuclei in the corpus callosum. MOG, GFAP and Ki67 were quantified in the corpus callosum between the midline and the point under the peak of the cingulum. At least three sections per mouse and three mice per condition were included in the quantification.

Custom array analysis of gene expression

RNA was isolated following a modified protocol from SABiosciences (Zhou et al., 2012). At least three mice were processed for each experimental condition and control group. Briefly, the corpus callosum was microdissected on ice, homogenized in 0.3 ml of TRIzol® (Invitrogen) and stored at −80℃. An additional 0.7 ml of TRIzol® was added to the samples when the RNA was isolated according to the manufacturer's instructions. The RNA was purified using the RT^2 QPCR-Grade RNA Isolation Kit (SABiosciences, PA-001). Purity readings were determined with a Nanodrop spectrophotometer (ThermoScientific). Samples were required to have A260/280 ratios above 2.0 and A260/230 ratios above 1.8. If necessary, samples were re-purified according to the SABiosciences protocol. Purified RNA samples were converted into cDNA (600 ng per reaction) using the RT First Strand Kit (SABiosciences, C-03) and used at 5 ng/10 μl in QPCR arrays.

A custom 386-well plate (SABiosciences) was designed for QPCR expression analysis of 96 genes relevant to characterization of astrogliosis and the cuprizone lesion environment (Supplementary Table S1 available at http://www.asnneuro.org/an/004/an004e100add.htm). On each plate, four different experimental conditions were run as a set of three disease time points and one control time point without cuprizone treatment. For each time point, cDNA was pooled from three mice of the same condition. Each experimental and control condition was run as technical triplicates on three different plates. Raw *Ct* (cycle threshold) values of 0 (failed reaction) and above 35 (below detection threshold) were excluded. Values from four housekeeping genes (Tbp, Hprt1, Actb and 18 sRNA) were used for loading normalization and quality screening for each sample. Relative changes across the disease time course and control ages were determined using the $\Delta\Delta Ct$ method relative to gene expression values for control mice (no cuprizone; 8 weeks of age matched to 0 week of cuprizone treatment). GenePattern 2.0 was used for analysis of relative mRNA expression patterns (Reich et al., 2006).

Statistical analysis

Prism 5.0 (GraphPad, Inc.) was used for graphing and statistical analyses. One-way ANOVA measures were used to determine significant differences between cuprizone treatment groups across the disease time course. Relative gene expression values were individually compared with a theoretical value of 1.0, for significance relative to no fold change, using a Student's *t*-test. Probability values of $P<0.05$ were considered significant.

RESULTS

Immunohistochemical confirmation of major disease stage of tissues used in analyses

Although cuprizone produces a relatively reproducible pattern of demyelination and remyelination, variations between anatomical sites and assessment methods lead to differences in comparison between studies, especially relative to remyelination (Armstrong et al., 2006; Kipp et al., 2011; Lindner et al., 2009; Mason et al., 2004; Xie et al., 2010). Therefore it is important to first illustrate the relative changes in myelination status across the time points to be used in the current study. Coronal sections through the caudal corpus callosum were immunostained for MOG, a myelin-specific glycoprotein, to estimate myelination status throughout the course of cuprizone treatment and recovery in the current study (Figure 1). MOG immunoreactivity is present throughout the extent of the corpus callosum in normal adult mice at 8 (start of cuprizone treatment; results not shown) and 26 weeks of age (end of time course; Figure 1A). The cuprizone treatment protocol resulted in consistent and extensive corpus callosum demyelination as shown at 6 and 12 weeks of cuprizone ingestion (Figures 1B and 1C). Myelin recovery throughout the corpus callosum indicated efficient spontaneous remyelination within 6 weeks of return to normal chow after a 6-week cuprizone treatment period (Figures 1D and 1F). In contrast, 12

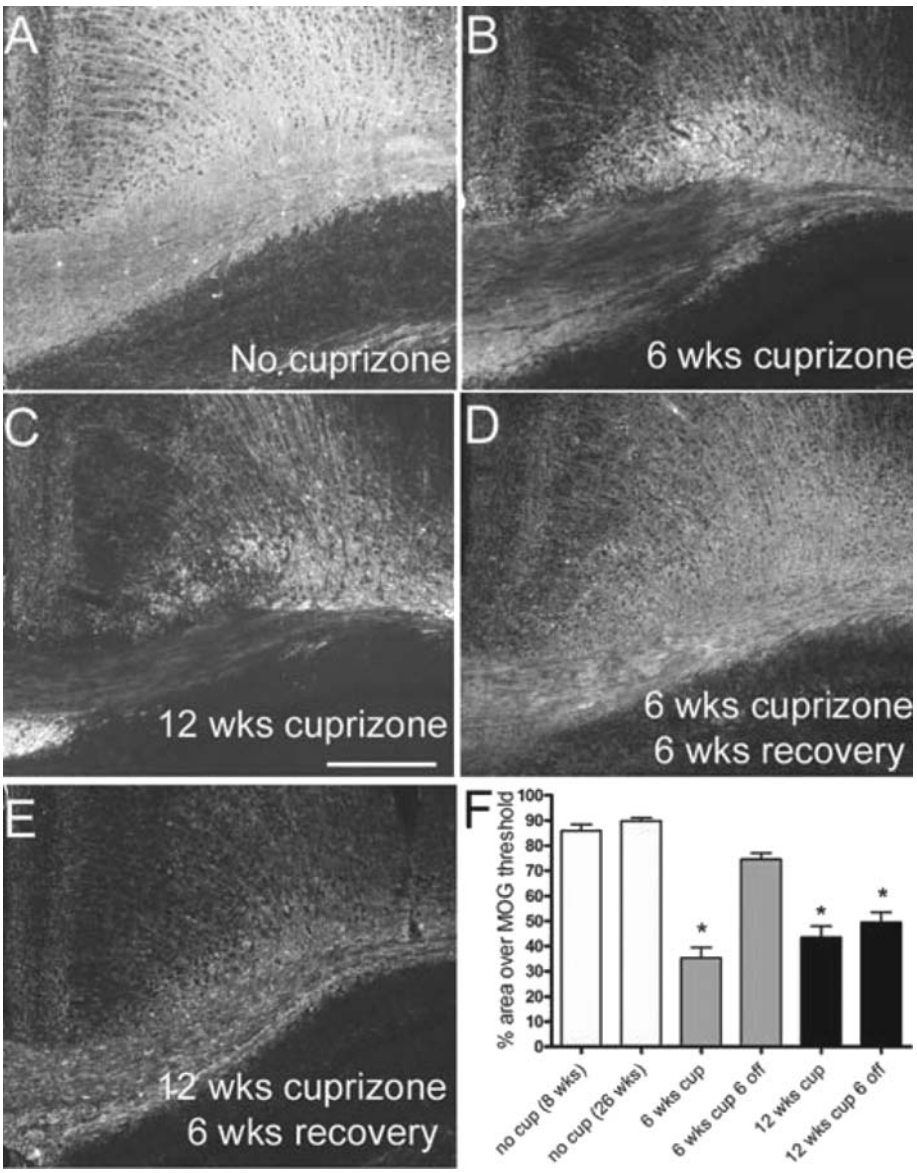

Figure 1 **Myelination status for acute and chronic cuprizone time points used to characterize astrogliosis**
Immunohistochemistry to detect MOG in coronal sections through the corpus callosum of mice without cuprizone (**A**; 26 weeks of age), or after cuprizone ingestion for 6 (**B**; acute) or 12 weeks (**C**; chronic) and a subsequent 6-week period after removal of cuprizone from the diet (**D**, **E**). Myelination status was estimated as the immunostained area of the corpus callosum (**F**). Compared with control mice at 8 ($n=8$) or 26 ($n=3$) weeks of age, myelination is significantly reduced after 6 ($n=5$) or 12 weeks ($n=8$) of cuprizone. The myelinated area returns to normal levels during the 6-week recovery period following 6 weeks of cuprizone ($n=5$) but not following 12 weeks of cuprizone ($n=8$). *$P<0.05$ compared with 26-week mice without cuprizone. Scale bar=100 μm for (**A**–**E**), shown in (**C**).

weeks of cuprizone feeding followed by a return to normal chow for 6 weeks resulted in partial, patchy remyelination (Figures 1E and 1F).

Quantitative analysis of the MOG immunostaining shows the reproducibility of these changes in myelination with each cuprizone paradigm (Figure 1F) and informs interpretation of the tissues used in the current studies for immunohistochemistry and QPCR. The myelination pattern shown here is consistent with our previous studies of demyelination and recovery with the same cuprizone protocol in C57BL/6 mice using MOG immunostaining and electron microscopy (Armstrong et al., 2006; Xie et al., 2010). The 6-week cuprizone treatment will be referred to as 'acute' demyelination, denoting a single transient episode of demyelination. The 12-week cuprizone treatment will be referred to as 'chronic' demyelination since these mice experience repeated demyelination and partial remyelination during prolonged cuprizone exposure (Armstrong et al., 2006; Mason et al., 2004).

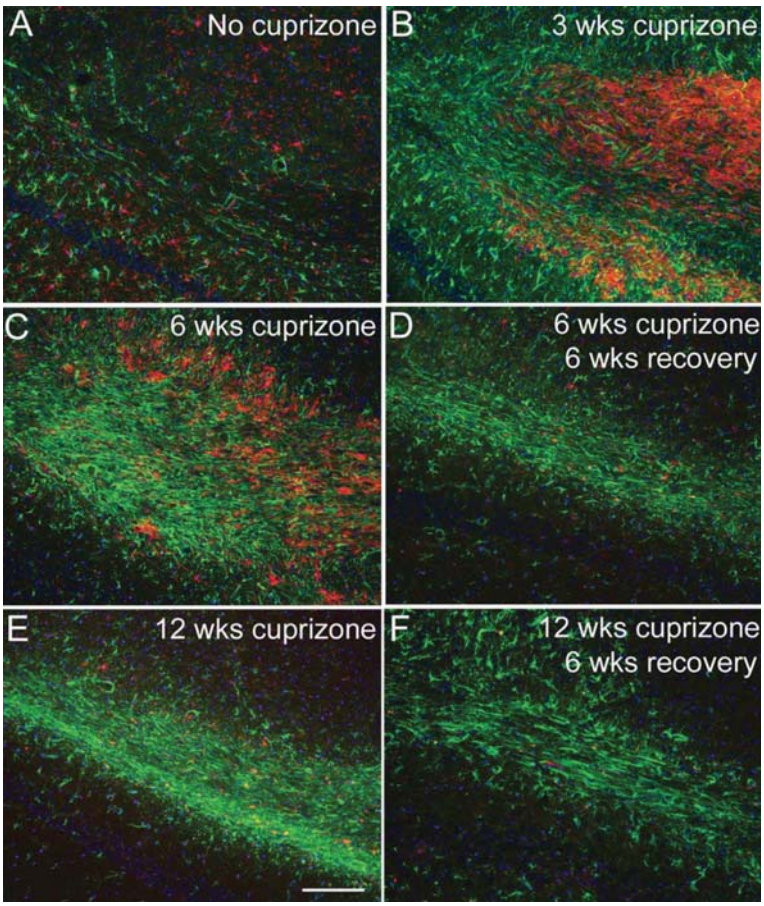

Figure 2 **Relationship of astrocyte reactivity and microglia activation during demyelination and recovery time periods**
GFAP (green) and CD11b (red) immunohistochemistry shows astrocyte reactivity and microglia/macrophage activation, respectively, after 3 weeks of cuprizone (**B**) in comparison with mice fed normal chow without cuprizone (**A**). CD11b immunoreactive cells are attenuated by 6 weeks of cuprizone (**C**) and then further reduced at the later time points either with continuous cuprizone (**E**; 12 weeks cuprizone) or during the recovery period following cuprizone for the acute (**D**; 6 weeks cuprizone followed by 6 weeks on normal chow) or chronic conditions (**F**; 12 weeks cuprizone followed by 6 weeks on normal chow). In contrast, strong astrocyte reactivity continues with continued cuprizone treatment as well as during the recovery periods. Scale bar shown for (**A**–**F**) shown in (**E**)=100 μm.

Relationship of astrocyte reactivity and microglia activation during demyelination and recovery time periods

We examined microglia and astrocyte populations as potential regulators of the lesion environment during the recovery period following cuprizone demyelination (Figure 2). Astrocytes and microglia were detected by immunoreactivity for GFAP and CD11b, respectively. In the corpus callosum of normal adult mice, GFAP is present in fine processes of distributed astrocytes and CD11b immunoreactivity is present on small microglia with branched processes (Figure 2A). After 3 weeks of cuprizone feeding, CD11b immunolabelled cells are present at a very high density in the corpus callosum (Figure 2B). At this early time point, astrocyte reactivity was also evident based on increased GFAP expression, hypertrophy, and disorganized process distribution (Figure 2B). CD11b immunoreactivity is attenuated at 6 weeks and further reduced at 12 weeks in contrast with the persistent astrocyte reactivity detected by GFAP immunohistochemistry (Figures 2C and 2E). Astrocyte reactivity continues to be evident at 6 weeks after the removal of cuprizone from the diet (Figures 2D and 2F), indicating that astrocyte reactivity may influence remyelination following acute and chronic demyelination.

Astrogliosis is induced for prolonged periods with cuprizone treatment

GFAP immunoreactivity was further examined for changes in astrocyte morphology and distribution (Figure 3) that indicate progressive stages of astrogliosis (Nash et al., 2011; Sofroniew and Vinters, 2010). In non-treated adult mice, astrocytes are distributed in discrete territories throughout the corpus callosum (Figure 3A). High GFAP expression in dense processes is prominent during cuprizone feeding

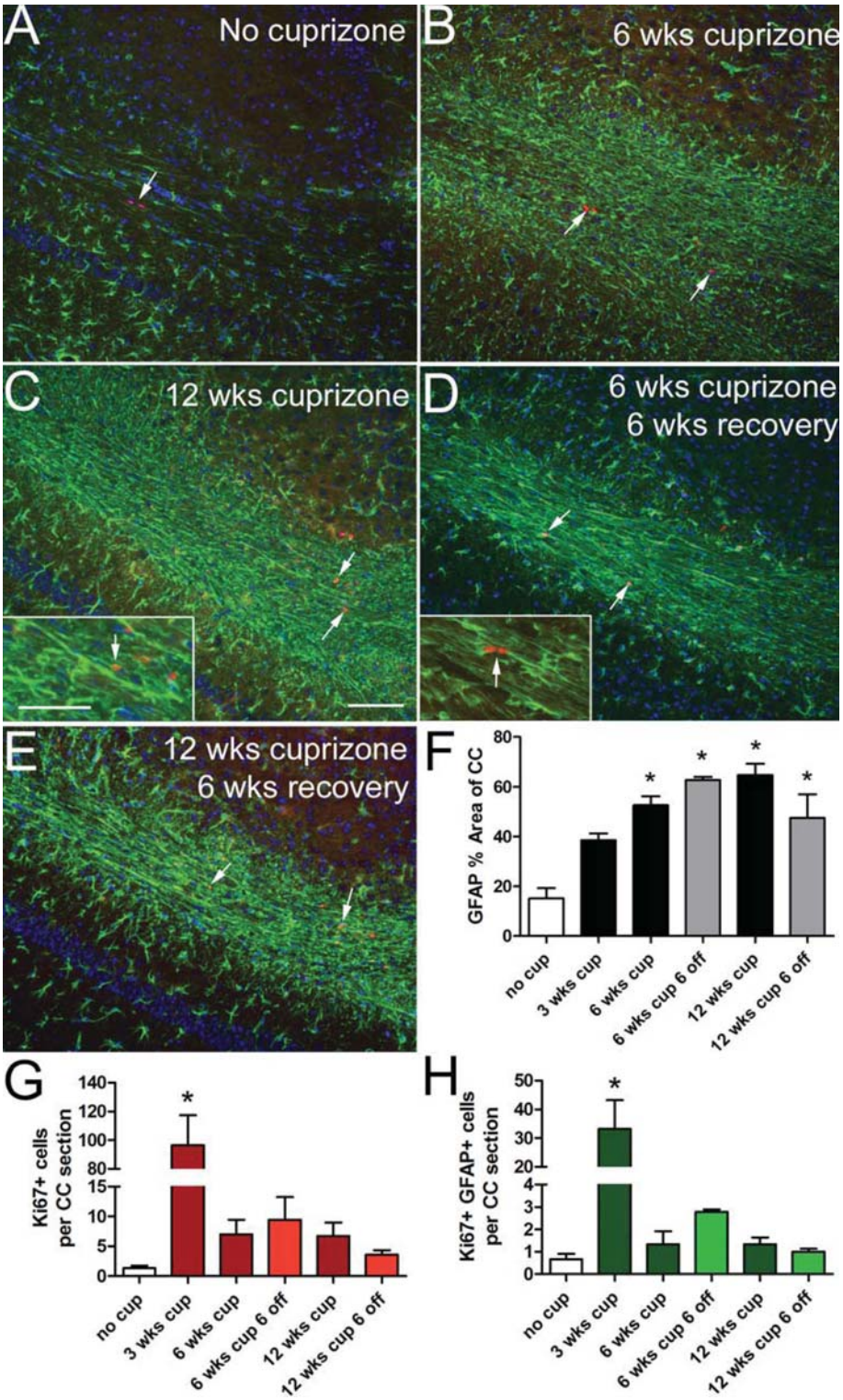

Figure 3 **Reactive astrogliosis and proliferation throughout chronic cuprizone treatment and recovery**

GFAP (green) immunohistochemistry shows increased immunoreactivity and altered astrocytic morphology after 6 (**B**) or 12 (**C**) weeks of cuprizone treatment in comparison with mice fed normal chow without cuprizone (**A**). These characteristics of reactive astrocytes continue to be prominent after a 6-week recovery period on normal chow following cuprizone treatment for 6 (**D**) or 12 weeks (**E**). Nuclear immunoreactivity for Ki67 (red; arrows) detects proliferating cells, some of which are clearly expressing GFAP (**C**, **D** inset arrows). Estimation of the percent area of the corpus callosum immunostained for GFAP shows increased reactive astrogliosis that is maintained throughout cuprizone treatment and during recovery on normal chow (**F**). Quantification of Ki67 positive cells shows significantly increased labelling at 3 weeks of cuprizone but proliferation is relatively mild across the later cuprizone time points (**G**). Quantification of cells double immunolabelled for GFAP and Ki67 shows a significant increase early during acute demyelination at 3 weeks of cuprizone treatment (**H**). *$P<0.05$ compared with control mice (8 weeks of age) without cuprizone ($n=3–4$ mice per time point). Scale bar shown for (**A–E**) shown in (**C**)=100 μm and inset=50 μm.

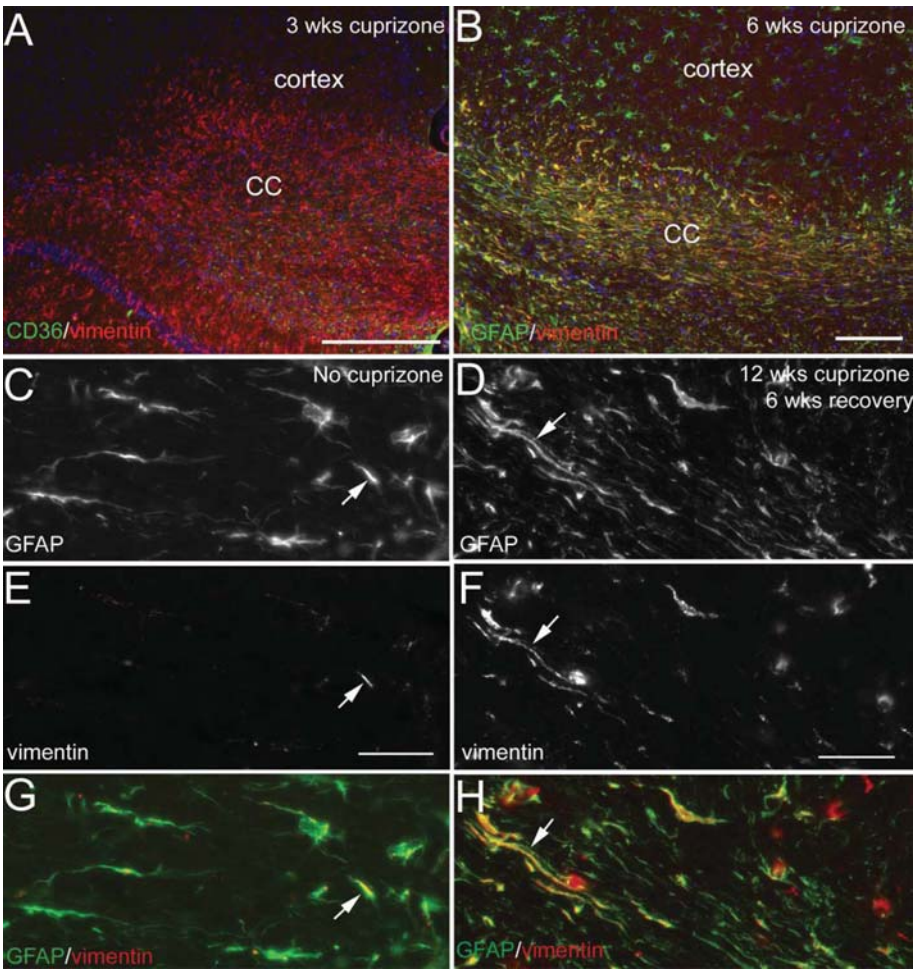

Figure 4 **Vim expression in astrocytes after chronic cuprizone**
(**A**) Strong Vim immunoreactivity is evident in the corpus callosum (CC) after 3 weeks of cuprizone. Double immunostaining with CD36, a marker of endothelial cells of blood vessels, accounts for only a subset of Vim expression. (**B**) Vim (red) and GFAP (green) double immunostaining shows extensive co-localization (yellow) in the corpus callosum at 6 weeks of cuprizone treatment. Astrocytes of the cerebral cortex have a lower level of Vim expression as compared with the adjacent corpus callosum. (**C**–**H**) Co-localization of Vim expression with GFAP continues through the recovery phase following chronic cuprizone demyelination. Regions of the corpus callosum in coronal tissue sections of mice without cuprizone treatment (**C**, **E**, **G**; 26 weeks of age) or after 12 weeks of cuprizone followed by 6 weeks on normal chow (**D**, **F**, **H**). Normal white matter astrocytes detected with immunolabelling for GFAP (**C** and green in **G**) do not express Vim (**E** and red in **G**), which is found in blood vessels and may co-localize with astrocyte processes that extend to blood vessels (arrows in **C**, **E**, **G**). In contrast, Vim (**D** and red in **H**) is co-localized with GFAP (**F** and green in **H**) in the cell body and processes (arrows in **D**, **F**, **H**) of elongated astrocytes during acute and chronic cuprizone treatment (not shown) that continues through the 6-week recovery period on normal chow (**D**, **F**, **H**). Scale bar for (**A**, **B**)=100 μm; (**C**, **E**, **G**) shown in (**E**)=50 μm; (**D**, **F**, **H**) shown in (**F**)=50 μm.

(Figures 3B and 3C). Extensive GFAP immunoreactivity in elongated processes persists during the recovery period on normal chow after either 6 or 12 weeks of cuprizone (Figures 3D, 3E and 3F).

GFAP immunolabelling was combined with detection of Ki67, a marker of cycling cells, to evaluate astrocyte proliferation as an additional factor indicating reactive astrogliosis (Nash et al., 2011; Sofroniew and Vinters, 2010). Overall cell proliferation is significantly increased only at the 3-week time point but is evident at each of the disease stages analysed in cuprizone-treated mice (Figure 3). Ki67 labelling is observed in cells that often appear as doublets consistent with cycling cells (Figures 3A and 3G). GFAP+ Ki67+ cells comprise a minority of the cycling cells, ranging from 29–40% across cuprizone time points (Figure 3H). Notably, astrocyte proliferation is significantly increased at 3 weeks of cuprizone, which is early during the acute demyelination period (Figure 3H).

Vim expression was also examined as an indicator of reactive astrocytes (Fuller et al., 2007; Nash et al., 2011). In the normal adult CNS, Vim is localized along blood vessels but is not expressed by astrocytes (Figure 4). Vim expression is co-localized with GFAP in reactive astrocytes throughout the cuprizone treatment period and continues during recovery on

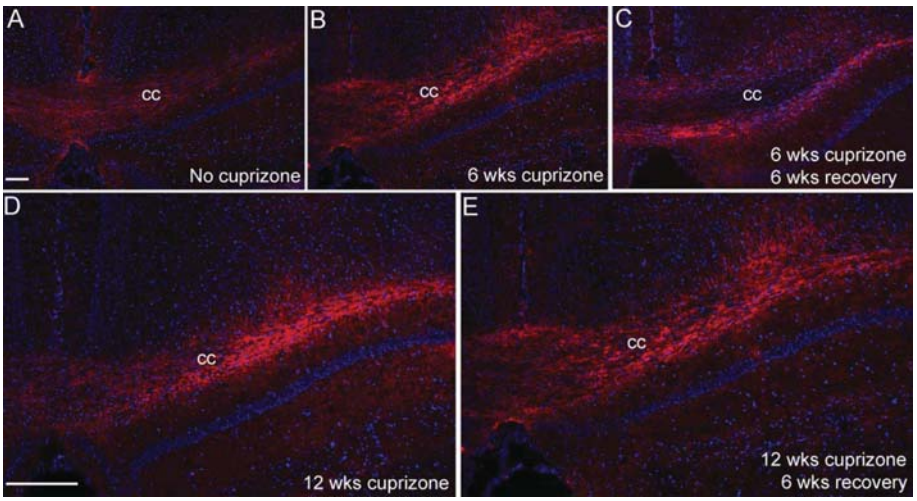

Figure 5 **CSPGs are increased in the corpus callosum after cuprizone treatment**
Immunohistochemistry of coronal sections through the CC (corpus callosum) immunostained for a pan-CSPG moiety with CS-56 antibody (red). CS-56 immunoreactivity is relatively low in the normal adult CC (**A**, 26 weeks) but increases with 6 (**B**) or 12 (**D**) weeks of cuprizone treatment. After the 6-week recovery period on normal chow, CS-56 immunoreactivity was more prominent after 12 weeks of cuprizone (**E**) than after only 6 weeks of cuprizone (**C**). Nuclei are stained with DAPI (4′,6-diamidino-2-phenylindole; blue). Scale bar for (**A**–**C**) shown in (**A**)=100 μm. Scale bar for (**D**, **E**) shown in (**D**)=200 μm.

normal chow (Figure 4). Vim up-regulation is most evident in the corpus callosum and much less pronounced in astrocytes of the adjacent cerebral cortex. GFAP and Vim intermediate filament proteins illustrate marked co-localization in astroglial processes elongated parallel to axons.

Expression of extracellular matrix molecules in cuprizone lesions indicates severe, diffuse astrogliosis without fibrotic scar formation

Astrogliosis can lead to deposition of extracellular matrix molecules to form a glial scar, which has been correlated with chronic forms of multiple sclerosis and implicated as a barrier to oligodendrocyte progenitor recruitment and/or differentiation after demyelination (Haist et al., 2012; Siebert and Osterhout, 2011; Siskova et al., 2006). CS-56 antibody was used to detect the GAG moiety of CSPGs. CS-56 immunoreactivity is low in the normal adult corpus callosum (Figure 5A) but is increased after cuprizone treatment (Figure 5). Fn1 immunoreactivity also accumulated in the corpus callosum during cuprizone treatment (Figure 6). However, collagen fibrils are not observed in chronic cuprizone lesions (Figure 7), which is consistent with a lack of blood–brain barrier disruption or overt tissue destruction (Sofroniew and Vinters, 2010).

QPCR array analysis throughout acute and chronic cuprizone treatment and recovery

QPCR was performed using a custom array to quantify gene expression patterns in the corpus callosum throughout the course of cuprizone treatment and recovery periods. Candidate genes were selected for two main purposes: (1) characterization of astrogliosis, in support of our immunohistochemical analysis, and (2) analysis of candidate signalling molecules in the lesion environment that may mediate astroglial reactivity or may impact remyelination. Supplementary Table S1 shows the full list of genes analysed along with gene names, abbreviations and sequence reference numbers. RNA isolated from the corpus callosum was analysed at 3-week intervals throughout the progression of cuprizone treatment for either 6 or 12 weeks. Importantly, the studies examined recovery periods after chronic cuprizone treatment to compare the expression pattern associated with limited remyelination with that of the more effective remyelination during recovery following acute cuprizone demyelination. Heat maps were generated to identify gene expression patterns that clustered with GFAP as a marker of astrogliosis (Figure 8).

The heat map for genes analysed throughout the acute (Figure 8A) and chronic (Figure 8B) cuprizone treatment and recovery time course show broad pattern similarity. Hierarchical clustering driven by GFAP identifies a set of genes with a similar pattern (above arrow in Figure 8). Overall, the genes clustering most closely with GFAP show relatively low expression (dark blue) in normal adult and undergo strong up-regulation during early demyelination (dark red at 3 weeks) with elevated levels continuing through 6 weeks and 12 weeks of cuprizone. Normalization during the recovery period appears less efficient following 6 weeks against 12 weeks of cuprizone. This heat map shows the correlation of GFAP with Vim and Fn1, supporting the immunostaining patterns shown above. Among the CSPGs examined, only Ptprz1 or DSD-1 proteoglycan, clustered with GFAP. DSD-1/Ptprz1 is a secreted, truncated splice variant of Ptprz1 (Faissner et al., 2006). Immunolabelling with a monoclonal antibody to

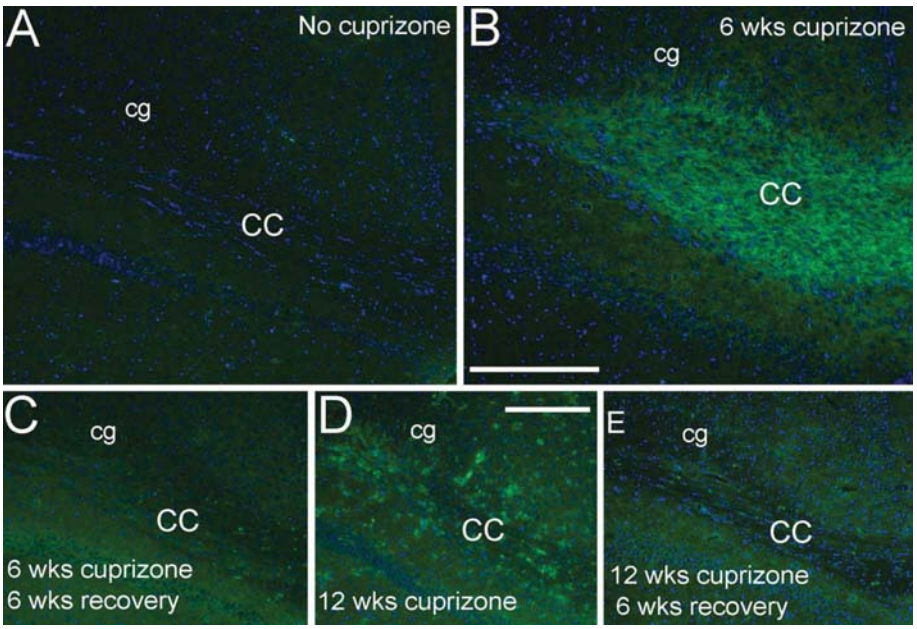

Figure 6 **Fn1 expression increases in the corpus callosum during cuprizone treatment**
Immunohistochemistry for Fn1 (green) and DAPI nuclear stain (blue) in control mice (**A**) shows minimal immunoreactivity in white matter of the CC (corpus callosum) or the cingulum (cg). Fn1 immunoreactivity in the CC is increased after 6 weeks of cuprizone (**B**) and present at lower levels by 12 weeks of cuprizone (**D**). The CC exhibits relatively minimal Fn1 immunoreactivity after a 6-week recovery period (**C**, **E**). Scale bars for (**A**, **B**) shown in (**B**)=200 μm. Scale bars for (**C**–**E**) shown in (**D**)=200 μm.

specifically detect DSD-1 confirmed that this specific CSPG isoform is expressed in lesions (Figure 9) in a pattern similar to the pan-CSPG antibody CS-56 (Figure 5).

Table 1 shows the specific fold-change values for these genes and other established indicators of reactive astrogliosis (Nash et al., 2011; Sofroniew, 2009; Zamanian et al., 2012). This QPCR array approach can reliably detect differences of greater than 1.33 fold (Hoebeeck et al., 2007). Significant but relatively mild up-regulation is observed for Sox9, a transcription factor associated with astrocyte synthesis of genes involved with the production of chondroitin sulphate side chains (Gris et al., 2007). Nes (nestin) is an intermediate filament protein that is up-regulated in astrocytes following some forms of CNS damage. With cuprizone treatment, Nes is only significantly increased at the 3-week time point, which is consistent with a previous immunohistochemical study of Nes expression (Gudi et al., 2011). TnC (tenascin C) is also often up-regulated in reactive astrocytes but is not strongly activated with cuprizone treatment. S100β and Glu1 (glutamine synthetase) are also associated with astrocytes but do not show an expression pattern that clusters with GFAP across either cuprizone time course. Genes associated with oligodendrocytes, Plp1 (proteolipid protein) and Gm98, serve to differentiate from the GFAP cluster and monitor oligodendrocyte loss and recovery (Figures 8A and 8B). Interestingly, CSPG4 (Figures 8A and 8B) also known as NG2, clusters more toward GFAP in the acute time course and more closely with Plp1 in the chronic time course. Supplementary Table S2 (available at http://www.asnneuro.org/an/004/an004e100add.htm) shows the fold-change values and statistical analysis for genes that did not cluster with GFAP, i.e. genes below the arrows in Figures 8(A) and 8(B).

In addition to characterization of astrocyte reactivity, our custom array examined candidate factors that can regulate astroglial reactivity as well as factors that can regulate oligodendrocyte lineage responses and remyelination. Analysis of this set of inflammatory and growth factor components facilitates an understanding of the lesion environment relative to astroglial reactivity across each disease time course. Table 2 shows the fold-change values of growth factor and inflammatory signalling components that clustered with GFAP across the acute and chronic demyelination and recovery time courses. Interestingly, the set of 22 candidate genes that correlate most closely with GFAP is the same in both the acute and chronic time courses. Among the genes clustering with GFAP (Figure 8), the fold change values and extent of correlation are highest during the acute demyelination and recovery time course (Figure 10). During the chronic time course, several growth factors, including FGF2 (fibroblast growth factor 2) and IGF-1 (insulin-like growth factor 1) maintain high GFAP correlations at or above the acute levels. However, TGFβ (transforming growth factor β) signalling components, BMP4 (bone morphogenetic protein 4) and LIF (leukaemia inhibitory factor) do not correlate as well with GFAP during the chronic time course.

Microglia are important contributors to the expression of inflammatory signals and growth factors in the cuprizone lesion environment. The microglial marker Itgam (integrin

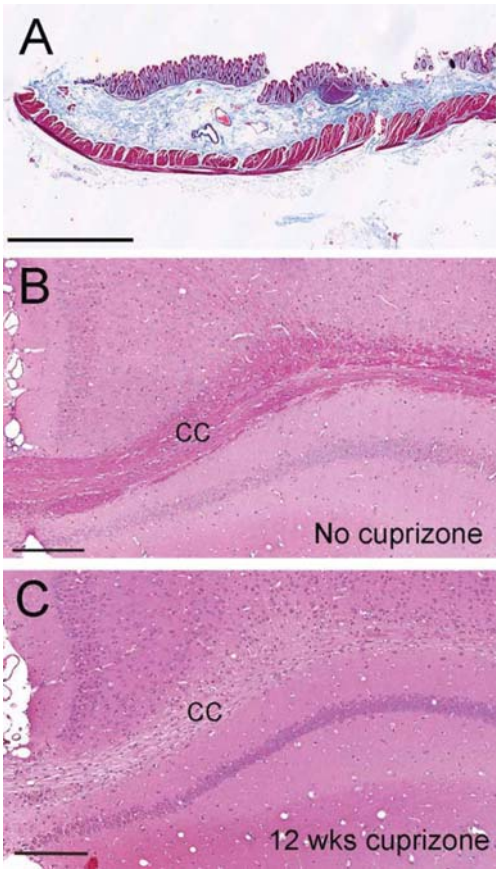

Figure 7 Chronic cuprizone treatment does not result in collagen deposition

Masson trichrome histological stain to detect collagen fibrils (blue) along with cytoplasm (pink) and muscle fibres (red) in a positive control section through a segment of intestine (**A**). In coronal sections through the corpus callosum (cc) from normal adult mice (**B**, 8 weeks) myelin also appears pink with the trichrome stain and blue nuclei are visible but collagen fibrils are not present. After 12 weeks of cuprizone (**C**) loss of the pink myelin staining is evident throughout the corpus callosum and nuclei are less organized but parenchymal or perivascular accumulations of collagen fibrils are not observed. Scale bars in (**A**–**C**)=200 μm.

alpha M or CDIIb) is increased during the initial episode of demyelination and also clusters with GFAP. However, Itgam and several genes clustering nearby (i.e. Itgam through BMP4) exhibit normalization during chronic cuprizone (blue shades at 12 weeks in Figure 8B) that is not observed for GFAP (red shades at 12 weeks in Figure 8B). These findings are consistent with the early-stage activation of microglia yet prolonged astrocyte reactivity that was observed in our immunohistochemical analysis of CD11b and GFAP expression (Figure 2).

DISCUSSION

The current study characterizes the expression of candidate regulatory molecules in cuprizone demyelinated corpus callosum to compare conditions of efficient with limited remyelination. Our analysis demonstrates that astrocyte reactivity persists during remyelination, in contrast with transient microglial activation, and therefore may be an important component of the lesion environment during the recovery period to influence remyelination efficiency. Cuprizone mediated demyelination in the corpus callosum results in severe, diffuse astrogliosis. Astrocytes exhibit increased expression of GFAP, Vim, Fn1 and CSPGs with a dense elaboration of processes and proliferation occurring during an early disease stage. Astrogliosis continues throughout the period of active demyelination. Prolonged astrocyte reactivity does not lead to progressive severity of astrogliosis or transition to a compact barrier or fibrotic scar. However, after removal of the demyelinating agent astrocyte reactivity does not normalize rapidly. Up-regulation of GFAP and Vim persists following either acute cuprizone demyelination in conjunction with extensive spontaneous remyelination or chronic demyelination with poor remyelination. Surprisingly, array expression analysis of candidate genes most closely correlated with GFAP in the corpus callosum tissues showed that the top 22 genes are shared between the acute and chronic time courses. The set of inflammatory mediators and growth factors that clusters with GFAP is most strongly up-regulated during acute demyelination.

Characterization of astrogliosis in the cuprizone demyelination model provides an important comparison with astrocyte reactivity stimulated by distinct mechanisms of CNS damage, such as penetrating injuries, ischaemia or inflammation. Astrocyte reactivity is heterogeneous with differential phenotypes dependent upon the inducing stimulus (Zamanian et al., 2012). Comparison of an ischaemic stimulus [MCAO (middle cerebral artery occlusion)] with an inflammatory stimulus [LPS (lipopolysaccharide) injection] showed differential expression among four established markers of reactivity in cortical astrocytes. MCAO induced elevation of GFAP, Vim, Nes and TnC while LPS elevated GFAP and Vim expression without up-regulation of Nes or TnC (Zamanian et al., 2012). In contrast with MCAO or LPS, the cuprizone model involves white matter astrocytes with demyelination as the predominant stimulus and occurs over a time course of several months. Astrocytes in the cortex exhibited cuprizone effects of hypertrophy and increased GFAP but these effects were less pronounced than in the corpus callosum (Figures 2–4), which is consistent with GFAP data from others (Buschmann et al., 2012; Gudi et al., 2011). Relatively mild changes were observed in the corpus callosum across the cuprizone time course for Nes and TnC as well as S100β and Glu1. The dramatic and prolonged elevation of GFAP and Vim in demyelinated white matter, as well as in cortex with diverse injury models (i.e. MCAO and LPS), shows that up-regulation of these intermediate filament proteins is a consistent marker of reactive astrocyte phenotypes.

Astrogliosis in multiple sclerosis lesions varies with autoimmune activity, blood–brain barrier integrity, location within the lesion area and disease duration (Lassmann, 2005; Wu and Raine, 1992). Astrocytes express GFAP and Vim in

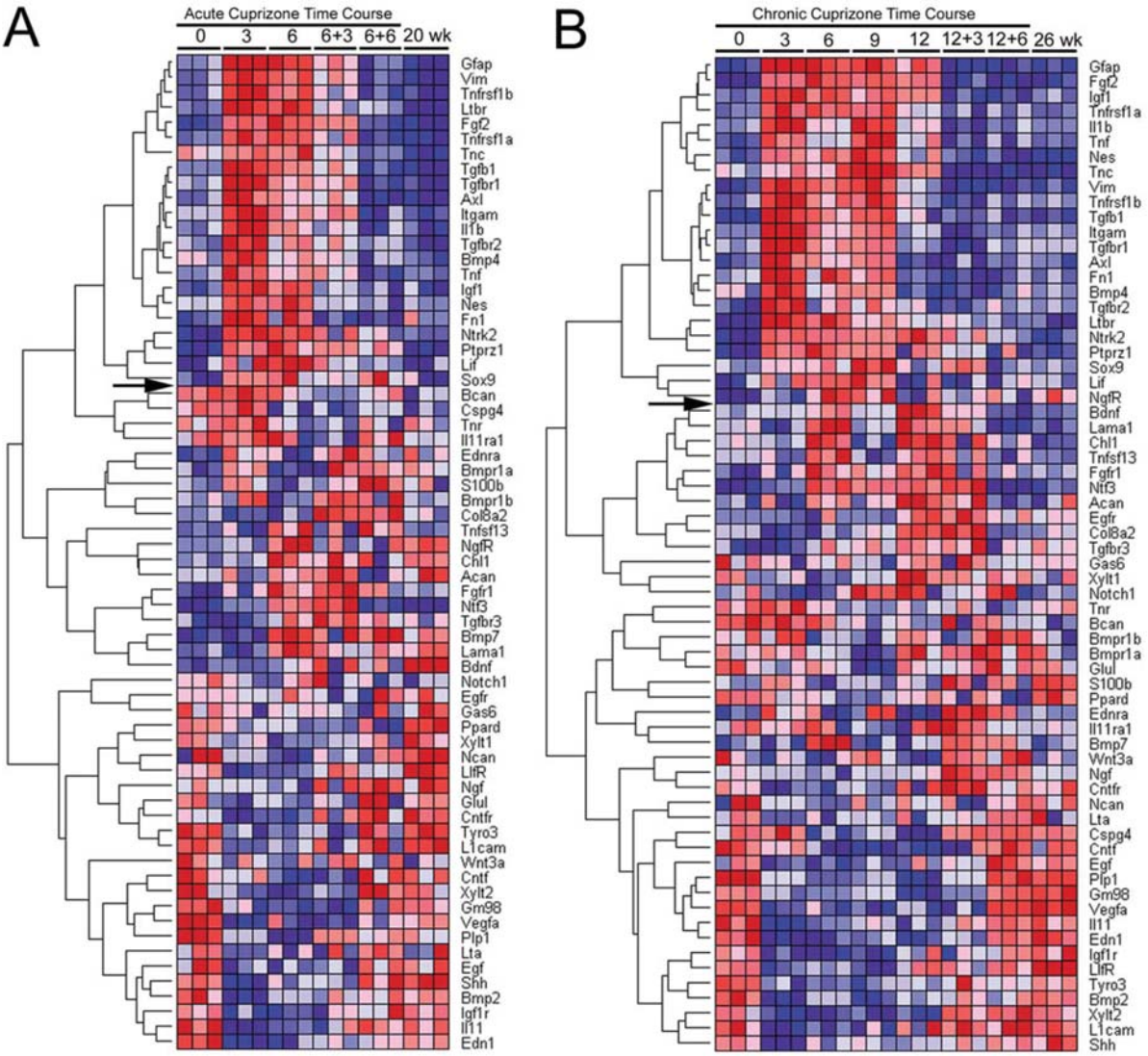

Figure 8 **QPCR custom array heat map of relative gene expression throughout the time course of acute (A) or chronic (B) cuprizone treatment and recovery**

RNA was isolated from the corpus callosum of mice at each time point shown along the top of the heat map. The time points are indicated as the number of weeks of cuprizone ingestion (0, 3, 6, 9 or 12) followed by the weeks on normal chow for recovery (+3 or +6). Results show fold-change values for each gene from triplicate PCR reactions which were each run on a separate plate. For each gene, relative expression levels are shown with the highest as dark red and the lowest as dark blue. Genes are hierarchically clustered based on correlation with expression of GFAP across each time course. Genes above the arrow on each heat map show a pattern similar to GFAP. The age-matched equivalent to the beginning of cuprizone treatment is shown as 0 week while the equivalent to the end of the time course of treatment and recovery is 20 week (**A**) for the acute and 26 week (**B**) for the chronic time course.

lesions across multiple sclerosis stages while scar forming astrocytes of chronic lesions exhibited antigenic changes that included increased expression of Nes and both TnC and TnR (Holley et al., 2003). However, another study showed demyelinated inactive multiple sclerosis lesions had increased levels of TnC but not TnR while neither tenascin was increased in demyelinated active lesions (Mohan et al., 2010). An increase of astrocytes expressing GFAP can be associated with actively demyelinating through early remyelinating multiple sclerosis lesions (Schonrock et al., 1998). Astrocytes undergoing proliferation, identified by Ki67, were relatively rare or absent in multiple sclerosis lesions but most frequently observed in early active and early remyelinating lesions (Holley et al., 2003; Schonrock et al., 1998), which is consistent with findings in the cuprizone model (Gudi et al., 2009) and current study (Figure 3). Accumulation of fibrillar collagen is associated with perivascular inflammation in multiple sclerosis lesions (Black et al., 2010; Mohan et al., 2010). The cuprizone lesions did not exhibit an astroglial scar interface with areas of fibrillar collagen. This result is consistent with the cuprizone mechanism of demyelination and indicates an absence of astroglial barrier formation that

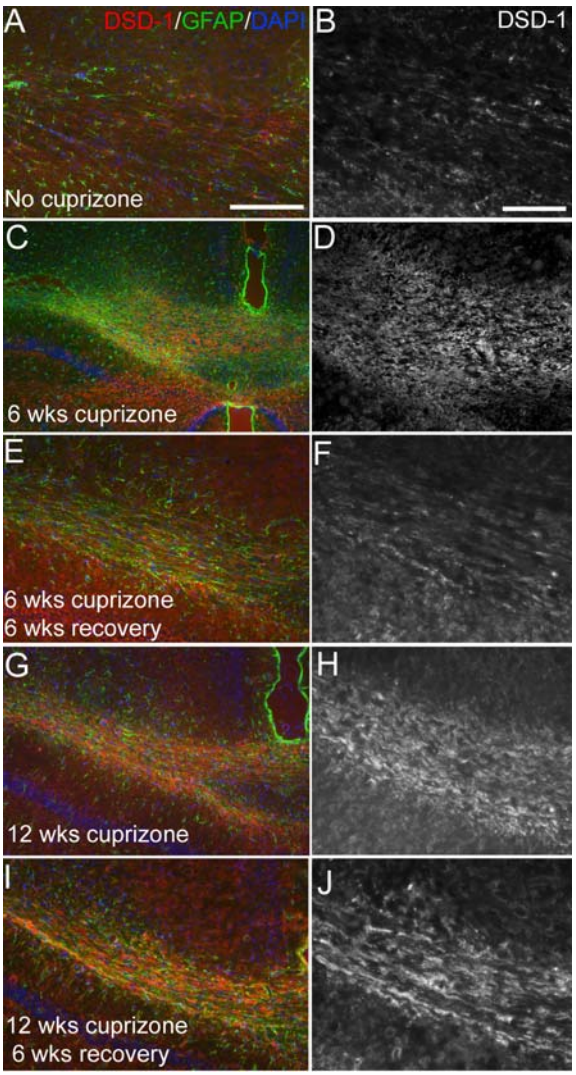

Figure 9 DSD-1 proteoglycan expression in lesioned corpus callosum
Immunohistochemistry of coronal sections through the corpus callosum showing labelling with a monoclonal antibody that is specific to the secreted, truncated variant of the Ptprz1 gene, DSD-1 proteoglycan (red) and GFAP as an indicator of astrocyte reactivity in lesion areas (green) along with DAPI nuclear stain (blue). DSD-1 immunoreactivity is shown at higher magnification in the greyscale images on the right. DSD-1 immunoreactivity is relatively low in the normal adult corpus callosum (**A**, **B**; 8 weeks) but increases with six (**C**, **D**) or 12 (**G**, **H**) weeks of cuprizone treatment. After the 6-week recovery period on normal chow, DSD-1 immunoreactivity was more prominent after 12 weeks of cuprizone (**I**, **J**) than after only 6 weeks of cuprizone (**E**, **F**). Scale bar for (**A**, **C**, **E**, **G**, **I**) shown in (**A**)=200 μm. Scale bar for (**B**, **D**, **F**, **H**, **J**) shown in (**B**)=50 μm.

would typically be associated with fibromeningeal cell infiltration during tissue destruction from trauma (Heck et al., 2007) or perivascular infiltration of immune cells in experimental autoimmune encephalomyelitis (Voskuhl et al., 2009). Chronic cuprizone lesions did show a dense network of thin astrocyte processes expressing GFAP and Vim similar to the astroglial morphology observed in chronic multiple sclerosis lesions (Black et al., 2010).

A major effect of astrocytes in a lesion environment is through expression of extracellular matrix molecules. Fn1 is normally present at low levels in the adult white matter but was increased in the corpus callosum during acute cuprizone demyelination. Deposition of Fn1 has been reported in active but not inactive multiple sclerosis lesions (Sobel and Mitchell, 1989; van Horssen et al., 2007). Fn1 in multiple sclerosis lesions was associated with extravasation from blood vessels or localized to astrocytes. Expression of Fn1 in white matter may inhibit oligodendrocyte process outgrowth and myelin sheath formation (Siskova et al., 2009).

CSPGs in glial scars inhibit axon regeneration (Bartus et al., 2012). Our array analysis indicated that Ptprz1 expression clustered with GFAP, in contrast with the other CSPGs examined (neurocan, Ncan; brevican, Bcan; aggrecan, Acan; NG2, CSPG4) or the xylotransferase enzyme isoforms (Xylt1, Xylt2) that initiate glycosylation of CSPGs. While NG2 is expressed by oligodendrocyte progenitor cells, astrocytes express each of the other CSPGs. Increased expression of CSPGs in reactive astrocytes may be mediated by BMP4 or TGFβ (Fuller et al., 2007; Susarla et al., 2011). Distinct CSPGs may have differential effects on oligodendrocyte lineage cell responses. Immunolabelling confirmed expression of phosphacan/DSD-1 in cuprizone lesions (Figure 9). Ptprz1 can be expressed by astrocytes, neurons and oligodendrocytes in the CNS (Faissner et al., 2006). Given that DSD-1 is a secreted protein, additional studies would be required to determine the cellular source(s) of DSD-1 during cuprizone demyelination and recovery. Both the pan-CSPG antibody CS-56 (Figure 5) and the DSD-1 antibody (Figure 9) consistently exhibited normalization of immunoreactivity following acute demyelination that was less evident following chronic demyelination. *In vitro* studies have indicated that neurocan and Ptprz1 inhibit oligodendrocyte progenitor cell differentiation (Siebert and Osterhout, 2011). However, Ptprz1 bound to contactin-1 on the surface of oligodendrocyte precursor cells inhibits proliferation and promotes differentiation into mature oligodendrocytes based on analysis of glial populations in *Ptprz* deficient mice (Lamprianou et al., 2011). Furthermore, *Ptprz*−/− mice exhibit impaired recovery from experimental autoimmune encephalomyelitis that is associated with increased apoptosis of oligodendrocytes (Harroch et al., 2002). In a lysolecithin mediated demyelination, *Ptprz*−/− mice exhibited accelerated axon loss (Huang et al., 2012). Therefore primary and secondary effects of *Ptprz* isoforms could be involved in neuron-glial interactions in lesions. In multiple sclerosis biopsies, Ptprz1 is expressed in lesion areas with cells expressing PLP, which together with the mouse studies indicates a potential role of Ptprz1 in oligodendrocyte survival and remyelination in demyelinating diseases (Harroch et al., 2002).

The current data from our QPCR analysis provides an important comparison of expression patterns during the recovery phase following acute against chronic demyelination. Our previous cuprizone QPCR study, using independent sets of mice, provided similar results for GFAP and Vim along

Table 1 **QPCR values for characterization of astrocyte reactivity**

The order of genes listed is according to the hierarchical clustering to GFAP shown for the chronic time course heat map. The values of 0, 3 and 6 weeks are included in both the acute (top row) and chronic (bottom row) time courses for each gene. The 9- and 12-week time points are not applicable (n.a.) to the acute time course. For the column labelled '20/26 week no cup', the upper rows show values for 20-week-old mice (non-treated mice age-matched to mice that were started on cuprizone at 8 weeks of age, then treated with cuprizone for 6 weeks and allowed to recover for 6 weeks). The bottom rows show values for 26-week-old mice (non-treated mice age-matched mice that were treated with cuprizone for 12 weeks and allowed to recover for 6 weeks). Values shown are fold change (means ± S.E.M.) calculated relative to 0 week (no cuprizone) condition. $n=3$ mice per condition with samples run across three plates as technical triplicates. ANOVA values are for comparison across all time points for a given gene. *Show significant changes ($P<0.05$) for individual time points using comparison to a theoretical mean of 1.000, i.e. null hypothesis for no-fold change. cup, cuprizone.

Gene	0 week no cup	3 week cup	6 week cup	9 week cup	12 week cup	3 week off	6 week off	20/26 week no cup	ANOVA *P* value
GFAP	1 ± 0.02	14.02* ± 0.87	7.64* ± 0.61	n.a.	n.a.	3.32* ± 0.09	2.96* ± 0.38	0.79 ± 0.11	<0.0001
				5.01* ± 0.78	6.35* ± 0.16	3.11* ± 0.26	1.30* ± 0.01	0.98 ± 0.09	<0.0001
Nes	1 ± 0.05	2.71* ± 0.06	1.95 ± 0.25	n.a.	n.a.	1.01 ± 0.05	1.10 ± 0.26	1.11* ± 0.02	<0.0001
				1.99 ± 0.24	1.50 ± 0.17	1.43 ± 0.12	0.94 ± 0.12	0.80* ± 0.03	0.0002
Tnc	1 ± 0.14	2.04 ± 0.27	1.52 ± 0.24	n.a.	n.a.	0.84* ± 0.03	0.89 ± 0.03	0.52* ± 0.05	0.0003
				1.81* ± 0.09	1.48 ± 0.13	0.79* ± 0.02	0.62* ± 0.06	0.441* ± 0.02	0.002
Vim	1 ± 0.11	14.70* ± 0.24	6.68* ± 0.14	n.a.	n.a.	3.39* ± 0.09	3.16* ± 0.32	1.20 ± 0.13	0.0001
				5.14* ± 0.69	4.00* ± 0.25	3.17* ± 0.08	1.63 ± 0.15	1.082 ± 0.05	<0.0001
Fn1	1 ± 0.04	3.26* ± 0.12	1.78 ± 0.34	n.a.	n.a.	0.96 ± 0.03	1.38 ± 0.11	1.59* ± 0.05	<0.0001
				1.13* ± 0.03	1.08 ± 0.03	1.17 ± 0.08	0.91 ± 0.08	0.86* ± 0.03	<0.0001
Ptprz1	1 ± 0.02	2.32* ± 0.12	1.91* ± 0.18	n.a.	n.a.	1.56* ± 0.06	1.87* ± 0.13	1.17 ± 0.07	<0.0001
				1.35* ± 0.08	1.50 ± 0.17	1.68* ± 0.04	1.27 ± 0.22	1.08 ± 0.05	<0.0001
Sox9	1 ± 0.06	1.62* ± 0.06	1.41 ± 0.16	n.a.	n.a.	1.19* ± 0.03	1.55 ± 0.14	1.16 ± 0.06	0.0043
				1.64* ± 0.09	1.13 ± 0.14	1.83* ± 0.14	0.85 ± 0.14	0.9 ± 0.02	0.0018

with multiple myelin genes as indicators of demyelination and remyelination (Zhou et al., 2012). However, acute and chronic recovery periods were not examined for comparison. Another group performed an Affymetix GeneChip array study of corpus callosum tissues following acute and chronic cuprizone but limited the recovery interval to only 2 days after return to normal diet (Kipp et al., 2011). The majority of hybridization array studies using the cuprizone model have focused on demyelination progression and the role of inflammatory components (Arnett et al., 2003; Jurevics et al., 2002; Morell et al., 1998). A QPCR study of a set of 13 candidate growth factors during acute demyelination showed results similar to the current study with significantly increased expression of TGFβ1, IGF-1, LIF and FGF2 (Gudi et al., 2011). Up-regulation of IGF-1 and FGF2 in microglia isolated during acute cuprizone demyelination complements *in situ* analysis, indicating expression of these growth factors in both microglia and astrocytes in demyelinating lesions (Armstrong et al., 2002, 2006; Gudi et al., 2011; Komoly et al., 1992; Messersmith et al., 2000). Thus, both astrocytes and microglia may contribute to the significant increase of expression of IGF-1 and FGF2 during demyelination. The presence of a specific growth factor and inflammatory signals in the lesion environment indicates potential activity, but extensive *in vivo* analyses are required to delineate functional effects on remyelination (Moore et al., 2011). Studies in the cuprizone model using transgenic or knockout mice indicate a role for IGF-1 in supporting oligodendrocyte survival and FGF2 as an inhibitor of oligodendrocyte progenitor differentiation (Armstrong et al., 2006; Mason et al., 2000; Murtie et al., 2005).

After 3 weeks of cuprizone, IL-1β (interleukin 1β) and TNFα (tumour necrosis factor α) are among the most highly up-regulated genes in our analysis (Table 2: Il1b, TNF). IL-1β and TNFα can be secreted by astrocytes or microglia and are involved in microglial activation (Nair et al., 2008). Microglial activation is strong during the initial phase of demyelination and much less robust during the chronic phase, as shown in Figure 2 and at additional time points in our previous study (Xie et al., 2010). Importantly, early microglial activation and release of inflammatory signals, such as IL-1β, can activate CD3 T-cells and initiate a cascade resulting in astrocyte secretion of TNFα, chemokines and ROS (reactive oxygen species) that induce demyelination at 3–4 weeks after initiation of cuprizone (Kang et al., 2012).

Together, these studies demonstrate several key findings that are important in the interpretation of environmental effects on remyelination capacity. Astroglial reactivity persists throughout the period of cuprizone feeding, in contrast with microglial activation which is more transient. The astroglial response is relatively similar during the recovery phase following acute or chronic demyelination even though the extent of remyelination is significantly different. Signals that may inhibit the efficiency of remyelination following chronic demyelination do not appear to be significantly increased after chronic demyelination. Therefore inhibitory molecules may simply have a greater effect when the pool of oligodendrocyte progenitors is reduced compared with the amplified progenitor pool that is available after acute demyelination (Armstrong et al., 2002, 2006; Mason et al., 2004).

Table 2 **QPCR values for candidate genes for characterization of the lesion environment relative to GFAP expression**

The order of genes listed is according to the hierarchical clustering to GFAP shown for the chronic time course heat map. The values of 0, 3 and 6 weeks are included in both the acute (top row) and chronic (bottom row) time courses for each gene. The 9- and 12-week time points are not applicable (n.a.) to the acute time course. For the column labeled '20/26 week no cup', the upper rows show values for 20-week-old mice (non-treated mice age-matched to mice that were started on cuprizone at 8 weeks of age, then treated with cuprizone for 6 weeks and allowed to recover for 6 weeks). The bottom rows show values for 26-week-old mice (non-treated mice age-matched to mice that were treated with cuprizone for 12 weeks and allowed to recover for 6 weeks). Values shown are fold change (means ± S.E.M.) calculated relative to 0 week no cuprizone condition. $n=3$ mice per condition with samples run across three plates as technical triplicates. ANOVA values are for comparison across all time points for a given gene. *Show significant changes ($P<0.05$) for individual time points using comparison with a theoretical mean of 1.000, i.e. null hypothesis for no-fold change. cup, cuprizone.

Gene	0 week no cup	3 week cup	6 week cup	9 week cup	12 week cup	3 week off	6 week off	20/26 week no cup	ANOVA *P* value
Fgf2	1 ± 0.04	5.16* ± 0.21	4.01* ± 0.36	n.a.	n.a.	2.45* ± 0.19	2.11* ± 0.21	1.35* ± 0.04	<0.0001
				2.63* ± 0.07	3.28* ± 0.06	2.04* ± 0.19	1.33 ± 0.10	1.12 ± 0.16	<0.0001
Igf1	1 ± 0.09	6.06* ± 0.50	3.26* ± 0.41	n.a.	n.a.	1.38* ± 0.07	2.09 ± 0.65	1.68 ± 0.41	<0.0001
				1.68* ± 0.05	2.58* ± 0.17	1.50 ± 0.23	0.82 ± 0.23	1.00 ± 0.04	<0.0001
Tnfrs1a	1 ± 0.06	5.97* ± 0.36	3.72* ± 0.18	n.a.	n.a.	1.86 ± 0.46	1.64 ± 0.19	1.15 ± 0.16	<0.0001
				2.37* ± 0.17	2.40 ± 0.38	1.71 ± 0.43	1.49 ± 0.19	0.81 ± 0.22	<0.0001
Il1b	1 ± 0.08	10.08* ± 0.57	3.13* ± 0.47	n.a.	n.a.	1.54 ± 0.15	2.26* ± 0.23	1.65* ± 0.02	<0.0001
				3.78* ± 0.62	2.90* ± 0.17	1.32 ± 0.41	1.517 ± 0.16	1.013 ± 0.17	<0.0001
Tnf	1 ± 0.28	22.8* ± 3.62	5.97* ± 0.69	n.a.	n.a.	4.07 ± 1.65	3.30 ± 0.77	3.65 ± 0.76	<0.0001
				12.33* ± 1.07	8.11 ± 1.87	4.68 ± 1.18	3.25 ± 1.37	1.6 ± 0.38	<0.0001
Tnfrs1b	1 ± 0.18	8.87* ± 0.24	3.877* ± 0.22	n.a.	n.a.	1.66 ± 0.45	2.14 ± 0.36	1.38* ± 0.03	<0.0001
				3.27* ± 0.24	2.7 ± 0.48	1.68 ± 0.36	1.72 ± 0.19	1.20 ± 0.08	<0.0001
Tgfb1	1 ± 0.08	5.59* ± 0.14	2.48* ± 0.26	n.a.	n.a.	1.54* ± 0.09	1.78 ± 0.19	1.11 ± 0.04	<0.0001
				2.17* ± 0.15	1.89* ± 0.20	2.16* ± 0.10	1.36 ± 0.20	0.98 ± 0.08	<0.0001
Itgam	1 ± 0.08	4.92* ± 0.27	2.03* ± 0.17	n.a.	n.a.	1.57* ± 0.03	1.2 ± 0.30	1.05 ± 0.06	<0.0001
				1.48* ± 0.06	1.49* ± 0.04	1.27 ± 0.16	1.17* ± 0.03	1.00 ± 0.05	<0.0001
Tgfbr1	1 ± 0.06	6.07* ± 0.19	2.21* ± 0.10	n.a.	n.a.	1.51 ± 0.21	1.37 ± 0.17	0.93 ± 0.03	<0.0001
				1.50 ± 0.17	1.43* ± 0.04	1.15 ± 0.05	1.41 ± 0.10	1.13 ± 0.11	<0.0001
Axl	1 ± 0.02	6.45* ± 0.65	2.36* ± 0.14	n.a.	n.a.	1.60* ± 0.06	1.7 ± 0.17	1.33 ± 0.13	<0.0001
				1.87* ± 0.09	1.46* ± 0.06	1.99 ± 0.31	1.37 ± 0.09	1.06 ± 0.08	<0.0001
Bmp4	1 ± 0.23	3.65* ± 0.06	1.37 ± 0.12	n.a.	n.a.	1.03 ± 0.13	1.11 ± 0.13	0.83 ± 0.08	<0.0001
				0.95 ± 0.14	0.92* ± 0.01	1.11 ± 0.10	0.93 ± 0.12	0.77* ± 0.03	<0.0001
Tgfbr2	1 ± 0.18	4.94* ± 0.33	1.91 ± 0.32	n.a.	n.a.	1.40* ± 0.06	1.89* ± 0.12	1.11* ± 0.02	<0.0001
				1.35 ± 0.23	1.72* ± 0.13	1.93* ± 0.10	1.61 ± 0.15	1.26* ± 0.05	<0.0001
Ltbr	1 ± 0.04	3.2* ± 0.12	2.10* ± 0.18	n.a.	n.a.	1.23* ± 0.05	1.68 ± 0.16	1.02 ± 0.08	<0.0001
				1.35* ± 0.05	1.68* ± 0.12	1.96* ± 0.12	1.38* ± 0.08	1.07 ± 0.15	<0.0001
Ntrk2	1 ± 0.05	2.06* ± 0.09	1.6-* ± 0.03	n.a.	n.a.	1.36 ± 0.13	1.47* ± 0.11	1.29* ± 0.03	<0.0001
				1.31* ± 0.05	1.69* ± 0.08	1.65* ± 0.11	1.31*0.06	1.05 ± 0.07	<0.0001
Lif	1 ± 0.22	3.33 ± 0.84	2.96* ± 0.15	n.a.	n.a.	1.70 ± 0.33	1.92* ± 0.17	1.44 ± 0.30	0.0118
				2.10 ± 0.65	1.53 ± 0.47	1.54 ± 0.37	1.37 ± 0.30	1.29 ± 0.13	0.048

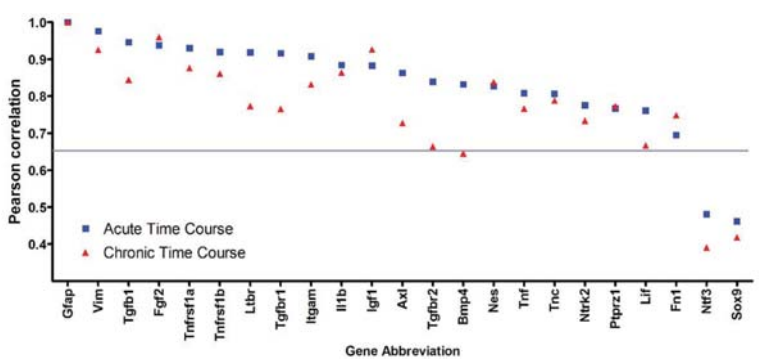

Figure 10 **Comparison of acute and chronic time courses based on the Pearson correlation with GFAP**

Genes that clustered with GFAP are ordered as in the heat map for the acute time course (Figure 7A). Correlations above 0.65 are considered significant (grey line) (Krasnov et al., 2005). Genes associated with characterization of astrocyte reactivity have a similar correlation across the acute and chronic time courses, as shown for Vim, Nes, TnC, Ptprz1 and Fn1. A similar tight correlation with GFAP for both time courses is found for FGF2 and IGF-1. However, many of the signalling components in the lesion environment show lower correlations with GFAP during the chronic time course, as shown for the TGFβ1, TGFβR1 and TGFβR2, BMP4 and LIF.

The cuprizone model has been extremely useful for identifying the specific molecular signals that regulate oligodendrocyte survival and the efficiency of oligodendrogenesis and remyelination (Deverman and Patterson, 2012; Gudi et al., 2011; Moore et al., 2011; VonDran et al., 2011; Zhou et al., 2012). The current studies now show the cuprizone model to be a relatively simple, reproducible model of persistent astrogliosis that continues during recovery following both acute and chronic demyelination. Prolonged astroglial reactivity from chronic cuprizone toxicity is not sufficient to lead to increased astrogliosis severity associated with barrier formation, fibrosis or sclerosis. These findings indicate that cuprizone demyelination may be an ideal system to test cellular and molecular factors that induce the endogenous astrocyte reactivity to progress to more severe astrogliosis and form non-remyelinating sclerotic areas of multiple sclerosis lesions.

ACKNOWLEDGEMENTS

We thank Dr Clifton Dalgard, Dr Stephen Rothwell and Dr Ravinder Pannu for help with the array studies. We thank Dr Aviva Symes and Dr Babette Fuss for advice in the immunohistochemistry protocols. We appreciate the helpful comments on the paper prior to publication from Dr Nicole Dobson and Dr Aviva Symes.

FUNDING

This work was supported by grants from the National Institutes of Health [grant number NS39293] and the National Multiple Sclerosis Society [grant number RG4224].

REFERENCES

Armstrong RC, Le TQ, Flint NC, Vana AC, Zhou YX (2006) Endogenous cell repair of chronic demyelination. J Neuropathol Exp Neurol 65:245–256.

Armstrong RC, Le TQ, Frost EE, Borke RC, Vana AC (2002) Absence of fibroblast growth factor 2 promotes oligodendroglial repopulation of demyelinated white matter. J Neurosci 22:8574–8585.

Arnett HA, Wang Y, Matsushima GK, Suzuki K, Ting JP (2003) Functional genomic analysis of remyelination reveals importance of inflammation in oligodendrocyte regeneration. J Neurosci 23:9824–9832.

Bartus K, James ND, Bosch KD, Bradbury EJ (2012) Chondroitin sulphate proteoglycans: key modulators of spinal cord and brain plasticity. Exp Neurol 235:5–17.

Black JA, Newcombe J, Waxman SG (2010) Astrocytes within multiple sclerosis lesions upregulate sodium channel Nav1.5. Brain 133:835–846.

Buschmann JP, Berger K, Awad H, Clarner T, Beyer C, Kipp M (2012) Inflammatory response and chemokine expression in the white matter corpus callosum and gray matter cortex region during cuprizone-induced demyelination. J Mol Neurosci 48:66–76.

Deverman BE, Patterson PH (2012) Exogenous leukemia inhibitory factor stimulates oligodendrocyte progenitor cell proliferation and enhances hippocampal remyelination. J Neurosci 32:2100–2109.

Faissner A, Heck N, Dobbertin A, Garwood J (2006) DSD-1-Proteoglycan/phosphacan and receptor protein tyrosine phosphatase-β isoforms during development and regeneration of neural tissues. Adv Exp Med Biol 557:25–53.

Fuller ML, DeChant AK, Rothstein B, Caprariello A, Wang R, Hall AK, Miller RH (2007) Bone morphogenetic proteins promote gliosis in demyelinating spinal cord lesions. Ann Neurol 62:288–300.

Gris P, Tighe A, Levin D, Sharma R, Brown A (2007) Transcriptional regulation of scar gene expression in primary astrocytes. Glia 55:1145–1155.

Gudi V, Moharregh-Khiabani D, Skripuletz T, Koutsoudaki PN, Kotsiari A, Skuljec J, Trebst C, Stangel M (2009) Regional differences between grey and white matter in cuprizone induced demyelination. Brain Res 1283:127–138.

Gudi V, Skuljec J, Yildiz O, Frichert K, Skripuletz T, Moharregh-Khiabani D, Voss E, Wissel K, Wolter S, Stangel M (2011) Spatial and temporal profiles of growth factor expression during CNS demyelination reveal the dynamics of repair priming. PLoS One 6:e22623.

Haist V, Ulrich R, Kalkuhl A, Deschl U, Baumgartner W (2012) Distinct spatio-temporal extracellular matrix accumulation within demyelinated spinal cord lesions in Theiler's murine encephalomyelitis. Brain Pathol 22:188–204.

Harroch S, Furtado GC, Brueck W, Rosenbluth J, Lafaille J, Chao M, Buxbaum JD, Schlessinger J (2002) A critical role for the protein tyrosine phosphatase receptor type Z in functional recovery from demyelinating lesions. Nat Genet 32:411–414.

Heck N, Garwood J, Dobbertin A, Calco V, Sirko S, Mittmann T, Eysel UT, Faissner A (2007) Evidence for distinct leptomeningeal cell-dependent paracrine and EGF-linked autocrine regulatory pathways for suppression of fibrillar collagens in astrocytes. Mol Cell Neurosci 36:71–85.

Hiremath MM, Saito Y, Knapp GW, Ting JP, Suzuki K, Matsushima GK (1998) Microglial/macrophage accumulation during cuprizone-induced demyelination in C57BL/6 mice. J Neuroimmunol 92:38–49.

Hoebeeck J, Speleman F, Vandesompele J (2007) Real-time quantitative PCR as an alternative to Southern blot or fluorescence *in situ* hybridization for detection of gene copy number changes. Methods Mol Biol 353:205–226.

Holley JE, Gveric D, Newcombe J, Cuzner ML, Gutowski NJ (2003) Astrocyte characterization in the multiple sclerosis glial scar. Neuropathol Appl Neurobiol 29:434–44.

Huang JK, Ferrari CC, Monteiro de Castro G, Lafont D, Zhao C, Zaratin P, Pouly S, Greco B, Franklin RJ (2012) Accelerated axonal loss following acute CNS demyelination in mice lacking protein tyrosine phosphatase receptor type Z. Am J Pathol, doi:10.1016/j.ajpath.2012.07.011.

John GR, Lee SC, Song X, Rivieccio M, Brosnan CF (2005) IL-1-regulated responses in astrocytes: relevance to injury and recovery. Glia 49:161–176.

John GR, Shankar SL, Shafit-Zagardo B, Massimi A, Lee SC, Raine CS, Brosnan CF (2002) Multiple sclerosis: re-expression of a developmental pathway that restricts oligodendrocyte maturation. Nat Med 8:1115–1121.

Jurevics H, Largent C, Hostettler J, Sammond DW, Matsushima GK, Kleindienst A, Toews AD, Morell P (2002) Alterations in metabolism and gene expression in brain regions during cuprizone-induced demyelination and remyelination. J Neurochem 82:126–136.

Kang Z, Liu L, Spangler R, Spear C, Wang C, Gulen MF, Veenstra M, Ouyang W, Ransohoff RM, Li X (2012) IL-17-induced Act1-mediated signaling is critical for cuprizone-induced demyelination. J Neurosci 32:8284–8292.

Kipp M, Gingele S, Pott F, Clarner T, van der Valk P, Denecke B, Gan L, Siffrin V, Zipp F, Dreher W, Baumgartner W, Pfeifenbring S, Godbout R, Amor S, Beyer C (2011) BLBP-expression in astrocytes during experimental demyelination and in human multiple sclerosis lesions. Brain Behav Immun 25:1554–1568.

Komoly S, Hudson LD, Webster HD, Bondy CA (1992) Insulin-like growth factor I gene expression is induced in astrocytes during experimental demyelination. Proc Natl Acad Sci USA 89:1894–1898.

Krasnov A, Koskinen H, Pehkonen P, Rexroad CE, 3rd, Afanasyev S, Molsa H (2005) Gene expression in the brain and kidney of rainbow trout in response to handling stress. BMC Genomics 6:3.

Lamprianou S, Chatzopoulou E, Thomas JL, Bouyain S, Harroch S (2011) A complex between contactin-1 and the protein tyrosine phosphatase PTPRZ controls the development of oligodendrocyte precursor cells. Proc Natl Acad Sci USA 108:17498–17503.

Lassmann H (2005) Multiple sclerosis pathology: evolution of pathogenetic concepts. Brain Pathol 15:217–222.

Lindner M, Fokuhl J, Linsmeier F, Trebst C, Stangel M (2009) Chronic toxic demyelination in the central nervous system leads to axonal damage despite remyelination. Neurosci Lett 453:120–125.

Lucchinetti C, Bruck W, Parisi J, Scheithauer B, Rodriguez M, Lassmann H (1999) A quantitative analysis of oligodendrocytes in multiple sclerosis lesions. A study of 113 cases. Brain 122:2279–2295.

Mason JL, Toews A, Hostettler JD, Morell P, Suzuki K, Goldman JE, Matsushima GK (2004) Oligodendrocytes and progenitors become progressively depleted within chronically demyelinated lesions. Am J Pathol 164:1673–1682.

Mason JL, Ye P, Suzuki K, D'Ercole AJ, Matsushima GK (2000) Insulin-like growth factor-1 inhibits mature oligodendrocyte apoptosis during primary demyelination. J Neurosci 20:5703–5708.

Matsushima GK, Morell P (2001) The neurotoxicant, cuprizone, as a model to study demyelination and remyelination in the central nervous system. Brain Pathol 11:107–116.

Messersmith DJ, Murtie JC, Le TQ, Frost EE, Armstrong RC (2000) Fibroblast growth factor 2 (FGF2) and FGF receptor expression in an experimental demyelinating disease with extensive remyelination. J Neurosci Res 62:241–256.

Mohan H, Krumbholz M, Sharma R, Eisele S, Junker A, Sixt M, Newcombe J, Wekerle H, Hohlfeld R, Lassmann H, Meinl E (2010) Extracellular matrix in multiple sclerosis lesions: fibrillar collagens, biglycan and decorin are upregulated and associated with infiltrating immune cells. Brain Pathol 20:966–975.

Moore CS, Abdullah SL, Brown A, Arulpragasam A, Crocker SJ (2011) How factors secreted from astrocytes impact myelin repair. J Neurosci Res 89:13–21.

Morell P, Barrett CV, Mason JL, Toews AD, Hostettler JD, Knapp GW, Matsushima GK (1998) Gene expression in brain during cuprizone-induced demyelination and remyelination. Mol Cell Neurosci 12:220–227.

Murtie JC, Zhou YX, Le TQ, Vana AC, Armstrong RC (2005) PDGF and FGF2 pathways regulate distinct oligodendrocyte lineage responses in experimental demyelination with spontaneous remyelination. Neurobiol Dis 19:171–182.

Nair A, Frederick TJ, Miller SD (2008) Astrocytes in multiple sclerosis: a product of their environment. Cell Mol Life Sci 65:2702–2720.

Nash B, Ioannidou K, Barnett SC (2011) Astrocyte phenotypes and their relationship to myelination. J Anat 219:44–52.

Plant SR, Arnett HA, Ting JP (2005) Astroglial-derived lymphotoxin α exacerbates inflammation and demyelination, but not remyelination. Glia 49:1–14.

Reich M, Liefeld T, Gould J, Lerner J, Tamayo P, Mesirov JP (2006) GenePattern 2.0. Nat Genet 38:500–501.

Schonrock LM, Kuhlmann T, Adler S, Bitsch A, Bruck W (1998) Identification of glial cell proliferation in early multiple sclerosis lesions. Neuropathol Appl Neurobiol 24:320–330.

Siebert JR, Osterhout DJ (2011) The inhibitory effects of chondroitin sulfate proteoglycans on oligodendrocytes. J Neurochem 119:176–188.

Siskova Z, Baron W, de Vries H, Hoekstra D (2006) Fibronectin impedes 'myelin' sheet-directed flow in oligodendrocytes: a role for a β 1 integrin-mediated PKC signaling pathway in vesicular trafficking. Mol Cell Neurosci 33:150–159.

Siskova Z, Yong VW, Nomden A, van Strien M, Hoekstra D, Baron W (2009) Fibronectin attenuates process outgrowth in oligodendrocytes by mislocalizing MMP-9 activity. Mol Cell Neurosci 42:234–242.

Sobel RA, Mitchell ME (1989) Fibronectin in multiple sclerosis lesions. Am J Pathol 135:161–168.

Sofroniew MV (2009) Molecular dissection of reactive astrogliosis and glial scar formation. Trends Neurosci 32:638–647.

Sofroniew MV, Vinters HV (2010) Astrocytes: biology and pathology. Acta Neuropathol (Berl) 119:7–35.

Susarla BT, Laing ED, Yu P, Katagiri Y, Geller HM, Symes AJ (2011) Smad proteins differentially regulate transforming growth factor-β-mediated induction of chondroitin sulfate proteoglycans. J Neurochem 119:868–878.

van Horssen J, Dijkstra CD, de Vries HE (2007) The extracellular matrix in multiple sclerosis pathology. J Neurochem 103:1293–1301.

Vana AC, Flint NC, Harwood NE, Le TQ, Fruttiger M, Armstrong RC (2007) Platelet-derived growth factor promotes repair of chronically demyelinated white matter. J Neuropathol Exp Neurol 66:975–988.

VonDran MW, Singh H, Honeywell JZ, Dreyfus CF (2011) Levels of BDNF impact oligodendrocyte lineage cells following a cuprizone lesion. J Neurosci 31:14182–14190.

Voskuhl RR, Peterson RS, Song B, Ao Y, Morales LB, Tiwari-Woodruff S, Sofroniew MV (2009) Reactive astrocytes form scar-like perivascular barriers to leukocytes during adaptive immune inflammation of the CNS. J Neurosci 29:11511–11522.

Wu E, Raine CS (1992) Multiple sclerosis. Interactions between oligodendrocytes and hypertrophic astrocytes and their occurrence in other, nondemyelinating conditions. Lab Invest 67:88–99.

Xie M, Tobin JE, Budde MD, Chen CI, Trinkaus K, Cross AH, McDaniel DP, Song SK, Armstrong RC (2010) Rostrocaudal analysis of corpus callosum demyelination and axon damage across disease stages refines diffusion tensor imaging correlations with pathological features. J Neuropathol Exp Neurol 69:704–716.

Zamanian JL, Xu L, Foo LC, Nouri N, Zhou L, Giffard RG, Barres BA (2012) Genomic analysis of reactive astrogliosis. J Neurosci 32:6391–6410.

Zhou YX, Pannu R, Le TQ, Armstrong RC (2012) Fibroblast growth factor 1 (FGFR1) modulation regulates repair capacity of oligodendrocyte progenitor cells following chronic demyelination. Neurobiol Dis 45:196–205.

Received 24 September 2012/accepted 26 September 2012

Published as Immediate Publication 2 October 2012, doi 10.1042/AN20120062